Interfacial energetics of two-dimensional colloidal clusters generated with a tunable anharmonic interaction potential

Elaa Hilou, Di Du, Steve Kuei, and Sibani Lisa Biswal*

Department of Chemical and Biomolecular Engineering, Rice University, Houston, Texas 77005, USA

Interfacial characteristics are critical to various properties of two-dimensional (2D) materials such as band alignment at a heterojunction and nucleation kinetics in a 2D crystal. Despite the desire to harness these enhanced interfacial properties for engineering new materials, unexpected phase transitions and defects, unique to the 2D morphology, have left a number of open questions. In particular, the effects of configurational anisotropy, which are difficult to isolate experimentally, and their influence on interfacial properties are not well understood. In this work, we begin to probe this structure-thermodynamic relationship, using a rotating magnetic field to generate an anharmonic interaction potential in a 2D system of paramagnetic particles. At low magnetic field strengths, weakly interacting colloidal particles form non-close-packed, fluidlike droplets, whereas, at higher field strengths, crystallites with hexagonal ordering are observed. We examine spatial and interfacial properties of these 2D colloidal clusters by measuring the local bond orientation order parameter and interfacial stiffness as a function of the interaction strength. To our knowledge, this is the first study to measure the tunable interfacial stiffness of a 2D colloidal cluster by controlling particle interactions using external fields.

I. INTRODUCTION

Novel two-dimensional (2D) materials have garnered significant interest due to their enhanced optical, electrical, chemical, and mechanical properties [1–4]. On the other hand, changes in molecular structure, chemical composition, or concentration can lead to unexpected phase transformations, which subsequently impact the performance of such materials. For example, it is known that a change in the temperature of a system results in thermal expansion; however, since this expansion directly affects both the thermodynamics and the kinetics of the system, it has been difficult to decouple the influence on the material's spatial configuration.

In an effort to investigate these phenomena, colloidal systems have been widely proposed as appropriate models for molecular systems. This has yielded new information concerning the thermodynamics and phase behavior of confined planar 2D systems [5–9], and more recently, newly investigated phenomena such as interfacial premelting with temperature-dependent colloidal particles [10] have shown the importance of interfacial dynamics to 2D material properties. Thus far, the majority of interfacial studies of colloidal systems utilize interactions represented by either charged particles, hard spheres, or depletion interactions [10–12]; however, many of the interesting properties of 2D molecular systems are governed by longer-range anharmonic interactions. Colloidal systems with tunable long-range interactions can be generated with magnetic and electric fields, but few studies have probed the resulting interfacial properties as a function of the interaction strength.

Recently, magnetic Janus particles in a rotating magnetic field have been shown to form colloidal crystals with a melted interface induced via a shear force [13], illustrating how dislocations in the bulk crystal migrate to the interface. In this work, we generate 2D colloidal clusters with a tunable long-range anharmonic interaction potential, and we characterize their energetics as well as their interfacial properties as a function of the interaction strength [see a video of the colloidal cluster shown in real time in the Supplementary Material (SM)] [14]. We find that the thermodynamic quantities are independent of the cluster size for the ranges used in this study (300 to 1500 particles). We begin by finding the excess internal energy of the clusters using a modified dipole model followed by a measurement of the interface fluctuations to calculate the excess free energy. These values can then be used in the Helmholtz free energy equation to obtain the excess entropy for each cluster. The finite size of the colloidal clusters allows us to simultaneously investigate both bulk and interfacial 2D properties. Of particular interest is understanding how increasing intermolecular interactions increases the configurational anisotropy of the interface, which in turn leads to variability in the line tension in crystallites. This has significant implications for highly correlated 2D materials where interface anisotropy impacts various transport properties within the material [15,16].

II. CLUSTER ENERGETICS

Under uniform magnetic fields, charged paramagnetic particles interact anisotropically with long-range dipolar attraction and short-range Derjaguin-Landau-Verwey-Overbeek (DLVO) repulsion. When placed in a high-frequency rotating magnetic field, the dipolar interaction is azimuthally averaged about each particle. This leads to a modified version of
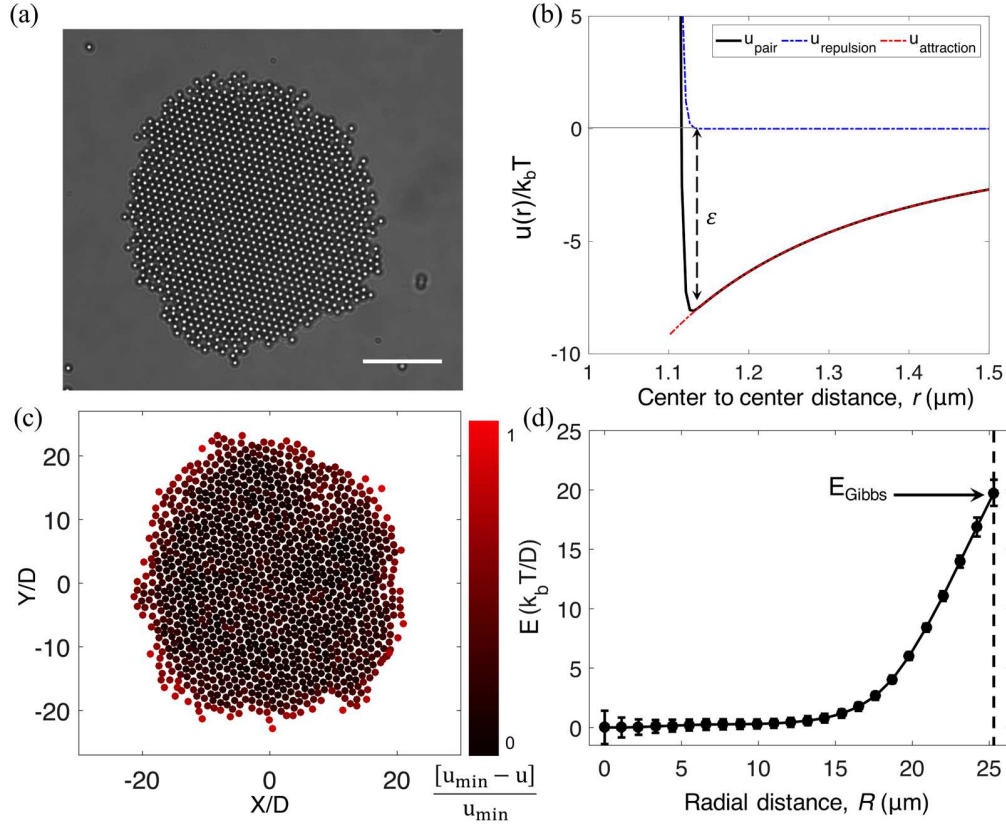
FIG. 1. Colloidal cluster under an externally applied magnetic field of 10 G. (a) Optical microscopy image of the colloidal cluster. Scale bar = 10 μm. (b) Interaction energy between particle pairs in the cluster ($u_\epsilon = -8.1k_bT$). (c) Potential energy distribution of particles in the cluster. Black particles represent the lowest energy state; red particles, high energies. (d) The change in energy potential across a cluster illustrates a concentrated bulk core and less stable interface.

the dipole model that is independent of the angle between particle pair and magnetic field vectors [17], which we use to characterize the internal energy of our system. This model has also been verified through experimental measurements using inverted Boltzmann analysis of the interparticle spacing (see Ref. [17] and SM [14] for the equations).

A high-frequency (20-Hz) rotating magnetic field is applied to assemble 2D colloidal clusters using a suspension of 1.1-μm-diameter carboxyl-coated paramagnetic particles which is placed in a flow cell between two pairs of orthogonal solenoid coils. Under an applied magnetic field, the particles begin to aggregate and assemble into 2D clusters that grow to be tens of microns in diameter [Fig. 1(a)]. In order to quantify the internal energy of each cluster, we begin by using a dipole model to calculate the internal energy of each particle [18]. Using this model, the net internal energy between the paramagnetic colloids can be approximated by the anharmonic interaction potential [Fig. 1(b)], $u(r) \sim \frac{A}{r^3}$, where r is the center-to-center distance between the particle pair and A is a function of the particle size, magnetic susceptibility, and magnetic field strength [18].

In order to compare this interaction potential to the thermal energy of the system, we write our energies in multiples of k_bT. The magnetic field strength selected for this set of experiments ranges from 8 to 12 G, which corresponds to pair potentials with well depths ($|u_\epsilon|$) ranging from $5.2k_bT$ to $11.7k_bT$.

Note that these values are reported as the inverse of the effective temperature, $T_{\text{eff}} = k_bT/u_\epsilon$, which is typically used in colloidal systems to more readily compare the magnitude of the interaction energy. In this study, T_{eff} ranges from 0.19 at 8 G to 0.085 at 11 G.

In a 2D system, the colloidal clusters prefer to form circular shapes to minimize their line tension, analogous to the minimization of interfacial tension in 3D. We define line tension, γ, as the mechanical work required to increase the interface length, which is a thermodynamic quantity that is independent of the molecular structure [19]. The cluster is a single-component system at quasiequilibrium with a constant temperature, T, cluster area, A, and number of particles, N. The configuration of a cluster at equilibrium is determined by minimization of the Helmholtz free energy, F, at the Gibbs interface [20]:

$$\frac{F^\sigma}{l} = \gamma + \sum_i (\mu_i \Gamma_i). \tag{1}$$

Here, F^σ/l is the excess Helmholtz free energy per unit length, l, i.e., the excess at the Gibbs dividing surface, σ, compared to the bulk value. At the interface, the Gibbs excess adsorption, Γ, is 0; thus, the line tension is equal to the Helmholtz free energy per length. In order to compare our energy calculations independently of the interfacial length and cluster size, we
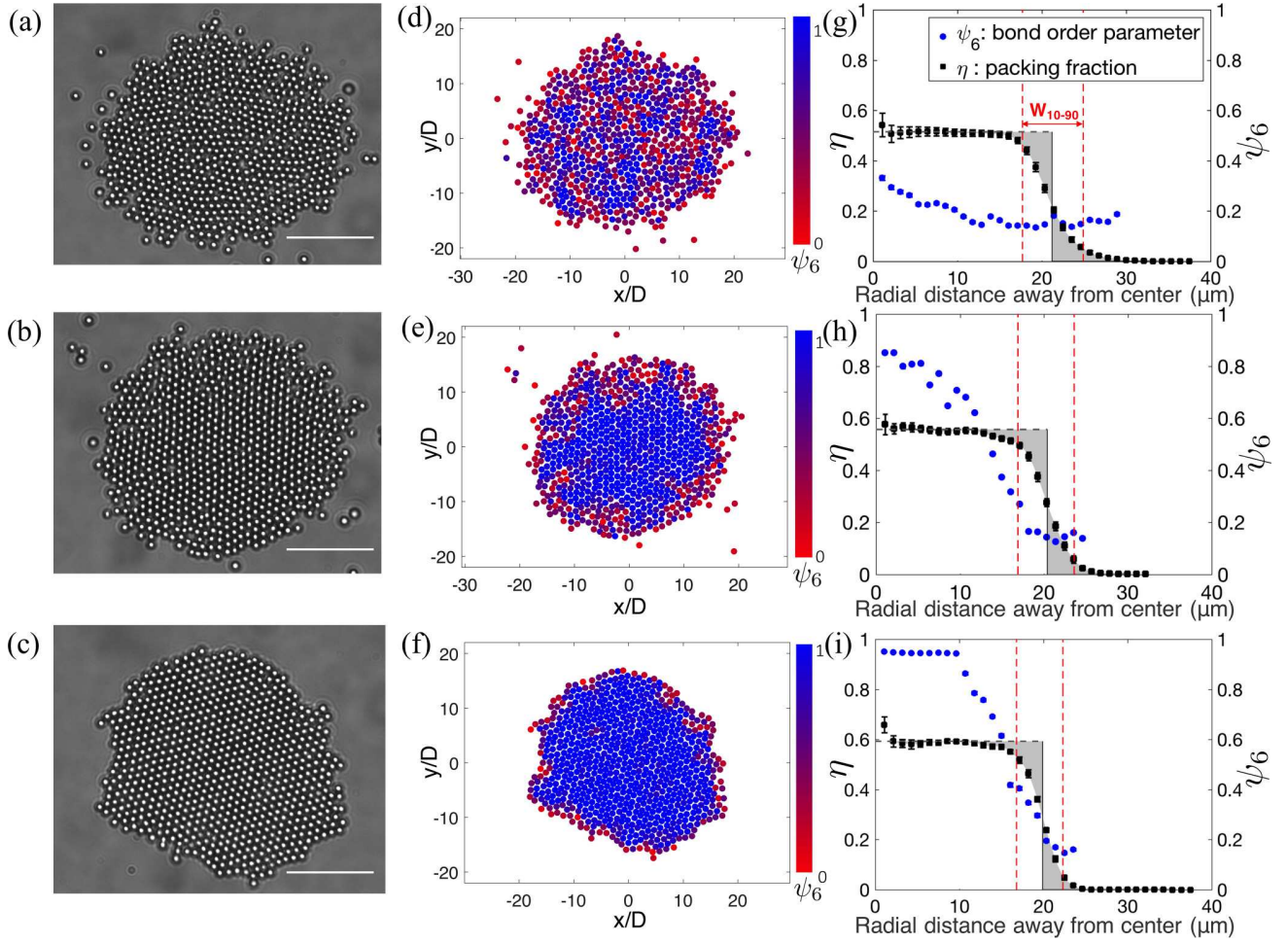
FIG. 2. Colloidal cluster under different magnetic field strengths. (a)–(c) Optical microscopy images of a colloidal cluster formed under magnetic fields of 8.5 G (a), 9 G (b), and 11 G (c), corresponding to pair potentials with magnitudes of $5.8k_bT$, $6.6k_bT$, and $9.8k_bT$, respectively. (d)–(f) Particle positions within the cluster for each of the three states based on their local orientation order parameter, ψ_6, value. ψ_6 ranges from 0 for low order (blue) to 1 for high order (red). (g)–(i) Plots of the packing density, η, and ψ_6 as a function of the distance away from the center of mass. Shaded gray areas represent the distance from the Gibbs dividing line to the bulk values of η of the two phases. Scale bar = 10 μm.

normalize our values by a unit length that divides the cluster into sector cells where the arc length of each cell is defined by a single particle (see SM [14]).

The second thermodynamic relationship to consider is the Helmholtz free energy; the difference between the potential energy of the system, U, and TS, where S is the entropy. By writing the equation in its excess form ($F^\sigma = U^\sigma - TS^\sigma$), and given F^σ and U^σ, we find the excess entropy of a cluster, a parameter that is experimentally challenging to obtain. Since the kinetic energy remains constant throughout the cluster, the excess kinetic energy goes to 0 and U^σ becomes solely governed by the anharmonic interaction potential between the particles.

Cluster stability is characterized by examining the potential energy distribution within a given cluster. Figure 1(c) shows a potential energy landscape for a given cluster and the energies of individual particles are illustrated using a bicolor gradient scheme. Note that since the energy calculation depends on the neighboring particles, any topological defects will also affect the energy of the neighboring particles. The radial change in the cluster's potential energy per unit length is defined

as E:

$$E(R) = U^\sigma/l = [\overline{u}(R) - \overline{u}_b]/l. \qquad (2)$$

Here, $\overline{u}_b$ is the energy in the bulk averaged over particles a distance R away from the center of the cluster. The particles in the bulk phase have the lowest potential energy ($u_{\min}$), whereas the energy of the particles increases when approaching the interface, as they begin to experience a change in the configuration of their neighboring particles as shown in Fig. 1(d).

III. CLUSTER TUNABILITY AND INTERFACIAL STIFFNESS

A. Cluster tunability

By increasing the strength of the magnetic field, and, by extension, the well depth of the particle pair potential, the clusters transition from a disordered fluidlike state to an ordered crystalline state. We quantify the change in the energetics and spatial characteristics of single 2D colloidal clusters using the analytical methods described in Sec. II. Figure 2 shows a cluster containing 710 to 730 particles at
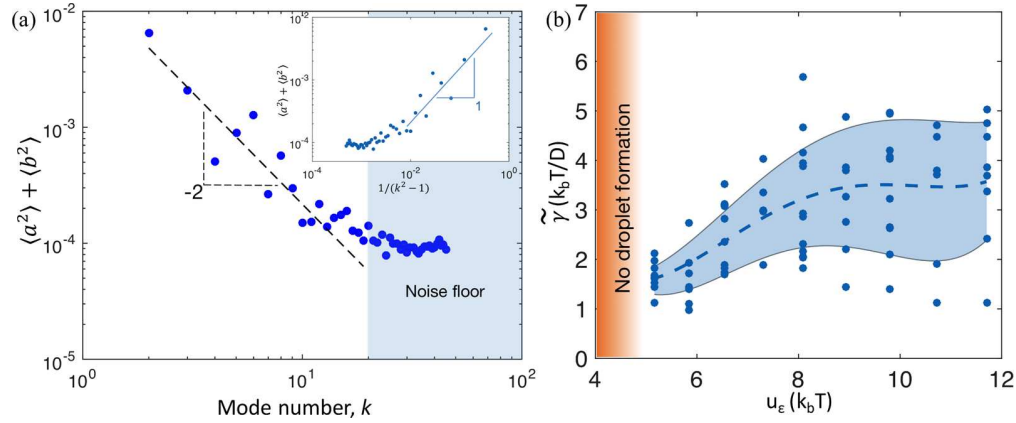
FIG. 3. Characterization of the clusters' interfacial fluctuation. (a) Correlation between the Fourier coefficients and the mode number reaching the noise floor at $k = 20$. Inset: The same data set, but with an x axis of $1/(k^2 - 1)$ to show that the slope is in agreement with Eq. (B2) in Appendix B. (b) Interfacial stiffness values at different particle pair interactions. Blue circles are experimentally obtained measurements of interfacial stiffness. Shaded blue area is the standard deviation of the data. Note that as u_ϵ increases anisotropy variations increase, leading to larger deviations in the interfacial stiffness.

interaction potentials of $5.8 k_b T$ [Fig. 2(a)], $6.6 k_b T$ [Fig. 2(b)], and $9.8 k_b T$ [Fig. 2(c)].

At the relatively low well depth of $5.8 k_b T$, particles throughout the entire cluster form a fluidlike disordered phase as shown in Fig. 2(d). Upon an increase in the potential well depth, a well-ordered microphase forms in the center of the cluster, surrounded by a disordered exterior layer. For clusters with more than 200 particles, the thickness of the disordered exterior becomes independent of the cluster size and is only dependent of the well depth. As the magnetic field is further strengthened, the crystalline microphase begins to grow towards the interface, resulting in a decrease in the thickness of the disordered boundary layer until it reaches a thickness of 1–2 particle diameters as shown in Fig. 2(f). The radial change in packing density, η, and ψ_6 are also plotted for each of the clusters [Figs. 2(g)–2(i)].

The characteristic interfacial width W_{10-90}, which scales with the particle diameter, D, was found using η and has also been shown to decrease with increasing magnetic field strength [21]. At well depths of $5.8 k_b T$, $6.6 k_b T$, and $9.8 k_b T$, W_{10-90} is $6.55D$, $6.09D$, and $5D$. The surface excess energy per unit length is calculated using Eq. (3) for each of the three states, and we find E to be $7.2 \pm 0.69 k_b T/D$, $14.2 \pm 1.21 k_b T/D$, and $22.4 \pm 1.25 k_b T/D$, respectively. As the cluster becomes less like a fluid and more like a crystal, it begins to deviate away from a circular shape to a more faceted structure. Such azimuthally anisotropic interfaces [Fig. 2(c)] lead to less accurate calculations near that region.

B. Interfacial stiffness

As previously stated, minimization of line tension causes the clusters to take on a circular shape. Although specific thermodynamic values can be determined as a function of u_ϵ, it is useful to generalize these interfacial energies in terms of interfacial stiffness, $\widetilde{\gamma}$, which is the sum of line tension and its second derivative with respect to the angle, θ, azimuthally normal to the interface ($\widetilde{\gamma} = \gamma + \frac{d^2\gamma}{d\theta^2}$), where the second term accounts for the orientation of the interface.

As shown in Fig. 2(a) the interface is isotropic at low magnetic field strengths. However, at high magnetic fields, shown in Fig. 2(c), the interface becomes anisotropic. Such is also the case for crystal-liquid interfaces [11,22] and crystal-crystal grain boundaries [23].

Interfaces corresponding to weakly associating particles fluctuate strongly compared to particles that are strongly associating. These radial fluctuations can be analyzed using Fourier methods to find the line tension [12,24,25]. For a two-dimensional system that is discrete and finite in size, one should account for the measurement uncertainty by estimating the modes at which we reach noise level. In order to estimate the Fourier modes that are insensitive to noise, we plot the Fourier coefficients (a_k, b_k) on a log-log scale as a function of the Fourier mode, k, as shown in Fig. 3(a). The plot has a slope of -2, showing an excellent agreement with the theoretical predictions in Refs. [24] and [26]. In our system, the noise level occurs at k higher than 15 to 20 modes.

As the interaction potential between the particles increases, $\widetilde{\gamma}$ increases and reaches a saturation value, as shown in Fig. 3(b). Interestingly, at the lowest field strengths the standard deviation in $\widetilde{\gamma}$ is small compared to that observed with stronger interaction potentials. At low $|u_\epsilon|$ where γ is the same along the interface, $\frac{d^2\gamma}{d\theta^2}$ term becomes negligible and $\widetilde{\gamma} \approx \gamma$. For higher potential energies, however, where the cluster orientation is anisotropic and differs from one crystallite to another, $\frac{d^2\gamma}{d\theta^2}$ becomes significant. For this reason, the variation in the interfacial stiffness increases as the clusters become more crystal-like as shown by the increasing scatter in Fig. 3(b). At well depths of $5.8 k_b T$, $6.6 k_b T$, and $9.8 k_b T$, $\widetilde{\gamma}$ is found to be $1.6 \pm 0.55 k_b T/D$, $2.5 \pm 0.66 k_b T/D$, and $3.7 \pm 1.5 k_b T/D$, respectively. Averaging measurements over 60 distinct clusters, the interfacial stiffness ranges between 1.73 ± 0.15 and $3.76 k_b T/D \pm 1.54 k_b T/D$. These values correspond to $(6.5 \pm 0.56) \times 10^{-15}$ and $(1.4 \pm 0.58) \times 10^{-14}$ when converted to units of J/m.

We compare our line tension measurements to other 2D colloidal systems [27–30], which mainly involve solid interfaces, and find that the values are of $\mathcal{O}(10^{-1} k_b T/D)$ or
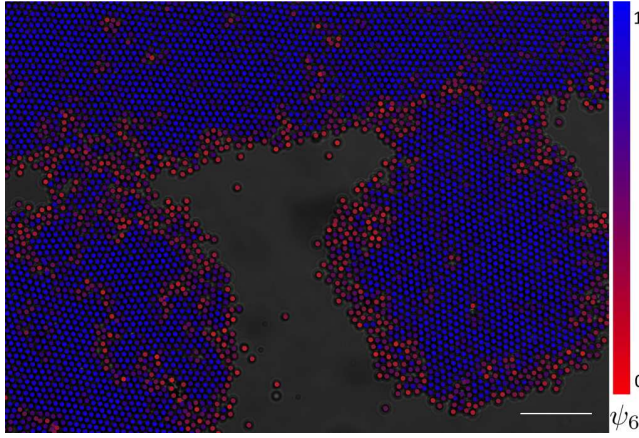
FIG. 4. Coalescence of two clusters into a large cluster under a field frequency of 20 Hz and field strength of 10 G. Scale bar = 10 μm.

FIG. 5. Micrographs of clusters coalescing taken over time at three interaction potentials: (a) $u_\epsilon = -5.2 k_b T$, (b) $u_\epsilon = -6.6 k_b T$, and (c) $u_\epsilon = -9.8 k_b T$. Images are color enhanced to indicate the bond orientation order parameter of each particle, and thus the level of disorder, in each of the three cases. See Supplemental Material for videos of their coalescence. Scale bar = 10 μm.

$\mathcal{O}(10^{-16} – 10^{-15}$ J/m). The line tensions were slightly lower than our liquidlike clusters and at least an order of magnitude less than our crystallites. We believe our system is able to reach values greater than typical colloidal models due to the influence of long-range interaction energy caused by the particles near the interface. Molecular dynamics simulations of 6-12 Lennard-Jones (LJ) systems, on the other hand, typically show line tensions ranging from $\mathcal{O}(10^{-12}$ J/m) to $\mathcal{O}(10^{-10}$ J/m) [31–33], which are orders of magnitude larger than our values. This is due to a number of dissimilarities between the two systems, such as length scale, entropic effects, and type of interaction driving phase separation [34].

Since γ represents F^σ / l, it is interesting to note that although we use two completely different methods to calculate F^σ / l (using Fourier expansion of the interfacial fluctuation) and U^σ / l (using the dipole model), both excess energies per unit length fall under the same order of magnitude.

Once we determine E and γ, we can find the excess entropy per unit length using the following relationship:

$$S^\sigma / l = -(\gamma - E)/T. \tag{3}$$

We find S^σ / l for each of the three states in Fig. 2 to be $5.6 k_b/D$, $11.7 k_b/D$, and $18.7 k_b/D$, respectively. Note that the excess entropy is an estimation and becomes less accurate at high fields since the excess Helmholtz free energy per length is equal to γ and not $\widetilde{\gamma}$. More exact calculation of thermodynamic parameters, such as the Helmholtz free energy, requires an accurate calculation of the spatial anisotropy of the cluster in order to obtain a better approximation for S^σ.

IV. CLUSTER COALESCENCE

Thus far we have focused on isolated quasistable clusters. Interesting interfacial dynamics can also be observed when clusters are near each other and begin to coalesce as shown in Fig. 4. Previous experiments [35,36] and simulations [37,38] have been performed to capture the coalescence of a variety of nanoscale and microscale systems to investigate changes in morphology and the formation of topological defects [39].
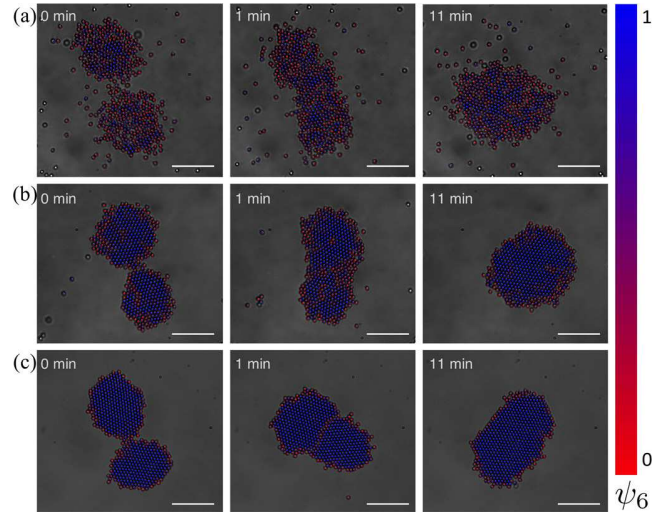
Here, we follow the dynamics of the colloidal clusters as they coalesce to form larger aggregates and qualitatively show the difference in clusters coalescing at low vs high field strengths. The coalescence mechanism can be described in four stages. First, clusters translate towards one another, resulting in a migration phase. Next, a neck of particles connects the clusters, as shown in Fig. 4. The resulting neck thickens and particles at the interface rearrange to move particles with ψ_6 closer to unity into the bulk phase while translating particles with low ψ_6 move to the interface. Finally, the merged cluster rearranges into a larger cluster that is once again quasistable with a circular morphology. For more crystalline clusters, grain boundaries are observed along the contact line between two clusters as they merge as shown in Fig. 4.

The relaxation and minimization of the potential energy of a cluster depend largely on the mobility of the constituent particles. As $|u_\epsilon|$ increases, the clusters are less mobile and therefore require more time to reach a global minimum potential energy. In Fig. 5, the coalescence of colloidal clusters is displayed over time at three interaction potentials. At low $|u_\epsilon|$, the larger cluster has a $\widetilde{\gamma}$ similar to that of the two original clusters. Coalescence-driven formation of topological defects is evident at higher interactions as shown in Figs. 5(b) and 5(c), and the resulting grain boundaries can range in thickness, depending on the strength of the interaction potential. At large enough $|u_\epsilon|$, the thickness of the disorder or grain boundary can be as small as 1 particle diameter [Fig. 5(c)]. These grain boundaries then migrate toward the interface and dissipate (see SM [14] for videos of the coalescence). The presence of topological defects in a crystalline system slows the progress toward a minimum free-energy state [40]. The coalescence of these crystallites therefore serves as a promising model for expanding studies that focus on the formation and migration of topological defects [27,41].

V. CONCLUSION

In summary, we have varied the strength of an anharmonic particle-particle interaction potential to characterize the changing interfacial properties of various 2D colloidal clusters. Structural parameters, such as the bond order parameter, are correlated with several thermodynamic quantities such as surface excess energy per unit length, surface excess entropy per unit length, and line tension. The tunability of the anharmonic potential presented here is ideal for study of long-range attractive 2D materials. This class of collective colloidal phenomena form the basis on which 2D interfacial dynamics can be explored.

APPENDIX A: EXPERIMENTAL DETAILS

The colloidal particles used in this study are $1.1 \pm 0.08 \ \mu$m paramagnetic carboxylated-coated MyOne Dynabeads (Invitrogen). A volume magnetic susceptibility of 1.4 is acquired as a result of iron oxide particles being embedded in a polystyrene matrix that makes up each particle. The stock suspension is washed and dispersed in an aqueous solution of 10 mM NaCl. A 0.035 vol% of the suspension is injected into a glass chamber that consists of two plasma-cleaned coverslips (Ted Pella, Inc.): one, 22×22 mm, acting as the top cover; and one, 24×40 mm, as the bottom surface. After the coverslips are plasma-cleaned, a 50-μm-thick Parafilm wafer is placed between the edges of the coverslips. The Parafilm acts as a spacer and, upon heating, as an adhesive to bind the coverslips. The suspension of paramagnetic particles of known concentration is added to the resulting chamber. The chamber is then sealed with epoxy followed by NOA 81 (Norland Optical Adhesive) to prevent the occurrence of any evaporation or capillary leakage. Since the particles have a density of 1.8 g/cm^3, they will sediment to the bottom of the chamber with a slight elevation due to the particles' being negatively charged, moving freely in the XY plane. Following the formation of the colloidal clusters, optical microscopy images are captured using a QICAM Fast 1394 camera and SimplePCI imaging software. Particle positions are determined using standard particle tracking algorithms [42].

APPENDIX B: INTERFACIAL STIFFNESS MEASUREMENT

Fluctuations of the interface are examined using Fourier analysis to quantify the interfacial stiffness as a function of the magnetic field strength. The correlation function in finite two dimensions entails finding the radial distance of the interface from the center of mass as a function of the angle θ that is normal to the interface. The fluctuations are then represented by the Fourier coefficients [24,26],

$$R(\theta) = R_0 \left[1 + a_0 + \sum_{k=1}^{\infty} a_k \cos(k\theta) + \sum_{k=1}^{\infty} b_k \sin(k\theta) \right],$$
(B1)

where R_0 is the equilibrium radius of the cluster and a_k and b_k are the Fourier coefficients for mode number k. The interfacial stiffness is correlated with the Fourier coefficients as [24]

$$\langle a_k^2 \rangle + \langle b_k^2 \rangle = \frac{2 k_b T}{\pi R_0 \widetilde{\gamma}} \left(\frac{1}{k^2 - 1} \right).$$
(B2)

The first 20 modes are considered, as further modes are indistinguishable from the noise floor as shown in Fig. 3(a).

APPENDIX C: ANALYTICAL APPROXIMATIONS

The potential energy of a colloidal cluster is determined by calculating the potential energy between each particle pair using a modified dipolar model [17]. The potential energy is approximated for a given particle within the cluster by summing the particle-pair interaction energy with every particle within 10 particle diameters. The interface is determined by calculating the packing fraction, η, of particles as a function of the distance from the cluster's center of mass. In order to generate a spatial profile of the particle density, the packing fraction is measured using annular disks in radial increments of one particle diameter. The position of the Gibbs dividing line is the location at which the integral of the density (or packing fraction) curve is equal to the spatial profile transitions from the bulk of the cluster to the dilute phase. A nonlinear regression is used to model the curve and find the distance at which the value falls from 90% to 10% [43], representing the interfacial width, W_{10-90} [21], and taken to be the limits of the integral. The surface excess energy is the excess potential energy at the Gibbs dividing line per unit length [$E(R_{\text{Gibbs}}) = U^\sigma / l$].

The local bond orientation order parameter [44], ψ_6, is used to characterize the structural order throughout each cluster,

$$\psi_6 = \left\langle \frac{1}{N} \left| \sum_i \frac{1}{N_n(i)} \sum_{k(i)} \exp(i 6 \theta_{ik}) \right| \right\rangle,$$
(C1)

where N is the total number of particles i in a radial region of interest, $N_n(i)$ is the total number of nearest neighbors for each particle i obtained using a Voronoi diagram, and θ_{ik} is the angle of the connecting vector between particle i and particle k relative to a reference line (positive x axis, in this case). The spatial profile is generated utilizing the same annulus used to calculate the packing fraction. The bond orientation order parameter quantifies the configuration in the interior domain of the cluster and follows the change in its crystallinity as the interaction energy between particles changes.

[1] F. Xia, H. Wang, D. Xiao, M. Dubey, and A. Ramasubramaniam, Nat. Photon. **8**, 899 (2014).

[2] X. Song, J. Hu, and H. Zeng, J. Mater. Chem. C **1**, 2952 (2013).

[3] D. Deng, K. Novoselov, Q. Fu, N. Zheng, Z. Tian, and X. Bao, Nat. Nanotechnol. **11**, 218 (2016).

[4] K. Liu and J. Wu, J. Mater. Res. **31**, 832 (2016).

[5] P. Pieranski, Phys. Rev. Lett. **45**, 569 (1980).

[6] G. Y. Onoda, Phys. Rev. Lett. **55**, 226 (1985).

[7] G. Leptoukh, B. Strickland, and C. Roland, Phys. Rev. Lett. **74**, 3636 (1995).

[8] C. P. Kelleher, R. E. Guerra, A. D. Hollingsworth, and P. M. Chaikin, Phys. Rev. E **95**, 022602 (2017).

[9] L. J. Moore, R. D. Dear, M. D. Summers, R. P. Dullens, and G. A. Ritchie, Nano Lett. **10**, 4266 (2010).

[10] B. Li, F. Wang, D. Zhou, Y. Peng, R. Ni, and Y. Han, Nature **531**, 485 (2016).

[11] J. Hernández-Guzmán and E. R. Weeks, Proc. Natl. Acad. Sci. USA **106**, 15198 (2009).

[12] D. G. Aarts, M. Schmidt, and H. N. Lekkerkerker, Science **304**, 847 (2004).

[13] J. Yan, S. C. Bae, and S. Granick, Soft Matter **11**, 147 (2015).

[14] See Supplemental Material at http://link.aps.org/supplemental/10.1103/PhysRevMaterials.2.025602 for more details.

[15] A. Allain, J. Kang, K. Banerjee, and A. Kis, Nat. Mater. **14**, 1195 (2015).

[16] X. Sun, H. Deng, W. Zhu, Z. Yu, C. Wu, and Y. Xie, Angew. Chem. Int. Ed. **55**, 1704 (2015).

[17] D. Du, D. Li, M. Thakur, and S. L. Biswal, Soft Matter **9**, 6867 (2013).

[18] E. E. Keaveny and M. R. Maxey, J. Comput. Phys. **227**, 9554 (2008).

[19] J. N. Israelachvili, *Intermolecular and Surface Forces* (Academic Press, New York, 2011).

[20] H.-J. Butt, K. Graf, and M. Kappl, *Physics and Chemistry of Interfaces* (John Wiley & Sons, New York, 2006).

[21] R. L. Davidchack and B. B. Laird, J. Chem. Phys. **108**, 9452 (1998).

[22] L.-H. Luu, G. Castillo, N. Mujica, and R. Soto, Phys. Rev. E **87**, 040202 (2013).

[23] T. O. Skinner, D. G. Aarts, and R. P. Dullens, Phys. Rev. Lett. **105**, 168301 (2010).

[24] E. Tüzel, G. Pan, and D. M. Kroll, J. Chem. Phys. **132**, 174701 (2010).

[25] R. E. Goldstein and D. P. Jackson, J. Phys. Chem. **98**, 9626 (1994).

[26] B. L. Stottrup, A. H. Nguyen, and E. Tüzel, Biochim. Biophys. Acta Biomembranes **1798**, 1289 (2010).

[27] A. E. González, Crystals **6**, 46 (2016).

[28] S. Auer and D. Frenkel, Phys. Rev. Lett. **91**, 015703 (2003).

[29] K.-Q. Zhang and X. Y. Liu, Nature **429**, 739 (2004).

[30] Z. Hu, P. Schall *et al.*, Phys. Rev. E **84**, 011607 (2011).

[31] J. H. Weijs, A. Marchand, B. Andreotti, D. Lohse, and J. H. Snoeijer, Phys. Fluids **23**, 022001 (2011).

[32] M. Shao, J. Wang, and X. Zhou, Sci. Rep. **5**, 9491 (2015).

[33] T. Werder, J. H. Walther, R. Jaffe, T. Halicioglu, and P. Koumoutsakos, J. Phys. Chem. B **107**, 1345 (2003).

[34] P. van der Schoot, J. Phys. Chem. B **103**, 8804 (1999).

[35] J. M. Yuk, M. Jeong, S. Y. Kim, H. K. Seo, J. Kim, and J. Y. Lee, Chem. Commun. **49**, 11479 (2013).

[36] J. Li, Z. Wang, C. Chen, and S. Huang, Sci. Rep. **4**, 5521 (2014).

[37] S. Hendy, S. A. Brown, and M. Hyslop, Phys. Rev. B **68**, 241403 (2003).

[38] L. Zhao and P. Choi, J. Chem. Phys. **120**, 1935 (2004).

[39] D. G. Aarts and H. N. Lekkerkerker, J. Fluid. Mech. **606**, 275 (2008).

[40] T. D. Edwards, Y. Yang, D. J. Beltran-Villegas, and M. A. Bevan, Sci. Rep. **4**, 6132 (2014).

[41] Z. Dai, S. Sun, and Z. Wang, Nano Lett. **1**, 443 (2001).

[42] J. C. Crocker and D. G. Grier, J. Colloid Interface Sci. **179**, 298 (1996).

[43] S. Patel, Y. Zhong, B. A. Bauer, and J. E. Davis, J. Phys. Chem. B **113**, 9241 (2009).

[44] D. R. Nelson and B. Halperin, Phys. Rev. B **19**, 2457 (1979).